Journal of Alloys and Compounds 513 (2012) 154–158

Contents lists available at SciVerse ScienceDirect

Journal of Alloys and Compounds

journal homepage: www.elsevier.com/locate/jallcom

Dielectric and optical properties of $BiFeO_3$–$(Na_{0.5}Bi_{0.5})TiO_3$ thin films deposited on Si substrate using $LaNiO_3$ as buffer layer for photovoltaic devices

Wei Qin, Yiping Guo*, Bing Guo, Mingyuan Gu

State Key Laboratory of MMCs, School of Materials Science and Engineering, Shanghai Jiaotong University, Shanghai 200240, China

ARTICLE INFO

Article history:
Received 16 August 2011
Received in revised form 4 October 2011
Accepted 4 October 2011
Available online 17 October 2011

Keywords:
Photovoltaic material
Sol–gel method
BFO–NBT ferroelectric thin film
Oriented films

ABSTRACT

Highly (100)-oriented $BiFeO_3$–$(Na_{0.5}Bi_{0.5})TiO_3$ thin films without undesirable phases were synthesized by chemical solution deposition. The preparation of $BiFeO_3$–$(Na_{0.5}Bi_{0.5})TiO_3$ sol and deposition procedure were studied. $BiFeO_3$–$(Na_{0.5}Bi_{0.5})TiO_3$ thin films were deposited onto SiO_2/Si substrates via a sol–gel method, with $LaNiO_3$ as buffer layer. X-ray diffraction analyses show that the $BiFeO_3$–$(Na_{0.5}Bi_{0.5})TiO_3$ films are highly (1 0 0)-oriented due to lattice match growth. Smooth surface with evenly distributed grains as small as about 50 nm were observed by scanning electron microscope. The dielectric and insulating characteristics against applied field, and optical properties were studied. It is found that the introduction of Ti^{4+} reduces the number of oxygen vacancy greatly and thus can suppress the leaking current. The film has a conspicuous absorption in the blue and green light region, and band gap of about 2.74 eV.

1. Introduction

$BiFeO_3$ (BFO) is a multiferroic material that simultaneously shows magnetic (antiferromagnetic), ferroelastic, and ferroelectric properties at room temperature. Because of its large polarization (~90 $\mu C\,cm^{-2}$), a high Curie temperature, G-type antiferromagnetic behavior, and its possible coupling with the magnetic moment at room temperature, BFO is one of the most studied multiferroic materials over the last few years [1–4]. Recently, the photoelectric and photovoltaic properties of BFO have attracted much attention mostly because it has a band gap in the visible range (~2.7 ev) [5–15], much lower than those of known ferroelectric photovoltaic materials such as $LiNbO_3$ and $Pb(Zr,Ti)O_3$ [16–18]. Extremely high open-circuit voltage [14], tunable voltage output [14], enhanced short circuit current density [12], and huge enhanced external quantum efficiency (QE) [15] have been reported on BFO bulk or thin films, which shows BFO is a promising candidate for applications in both the novel optoelectronic and the solar energy devices.

The photovoltaic efficiency of polycrystalline films is much smaller than that of epitaxial films [7]. However, polycrystalline BFO films are still very promising for practical applications due to their low cost and simple fabrication process. It is obvious that the leakage current has a significant effect on photovoltaic effect. In the polycrystalline BFO films, secondary phases leading to defects and nonstoichiometry easily result in high leakage current. Electrical poling becomes difficult due to higher conductivity, which will destroy the rotation of domain and then become hard to obtain photovoltaic effect. Many studies have focused on BFO films with ion substitutions or BFO solid solution films to enhance electric properties [8,19,20]. In the present work, we have prepared BFO solid solution thin films with $Na_{0.5}Bi_{0.5}TiO_3$ (NBT).

NBT is a lead-free perovskite ferroelectric with rhombohedral symmetry and space group *R3c*, which is similar to that of BFO [21]. It is a strong ferroelectric with a remanent polarization and coercive field of 38 $\mu C\,cm^{-2}$ and 73 $kV\,cm^{-1}$, respectively. Recent researchers [22,23] indicated that a pure perovskite structure can be obtained in $BiFeO_3$–$(Na_{0.5}Bi_{0.5})TiO_3$ (BFO–NBT) ceramic compounds, which is possibly suitable for depositing the corresponding films. Since orientation has a great impact on the domain structure as well as the optical and ferroelectric properties, it is therefore desirable to analyze the structural, optical, and ferroelectric properties of oriented thin films. In this paper, we report on the synthesis of highly oriented BFO–NBT thin films on Si substrates using $LaNiO_3$ (LNO) as buffer layer, and the electrical, dielectric, and optical properties of the thin films.

2. Experimental

$LaNiO_3$ thin films as bottom electrode were deposited on Si substrates with reference to a reported method [24]. $(1-x)$BFO–xNBT thin films with $x = 0.05$, 0.10, and 0.15 were prepared on Si substrates by a sol–gel process [25,26]. The BFO–NBT precursor solutions were prepared using titanium isopropoxide $[Ti[OCH(CH_3)_2]_4]$, bismuth nitrate $[Bi(NO_3)_3{\cdot}5H_2O]$, iron nitrate $[Fe(NO_3)_3{\cdot}9H_2O]$, and sodium nitrate $[NaNO_3]$ as starting materials. First, titanium isopropoxide, sodium nitrate, and bismuth nitrate (5% bismuth excess to compensate the Bi loss) were mixed and dissolved in acetylacetone together with 2-methoxyethanol by stirring for 20 min at room temperature. Iron nitrate was then dissolved in the solution above under constant stirring. Precipitation could not be avoided until ethanolamine and acetic

* Corresponding author.
E-mail address: ypguo@sjtu.edu.cn (Y. Guo).

0925-8388/$ – see front matter © 2011 Elsevier B.V. All rights reserved.
doi:10.1016/j.jallcom.2011.10.011

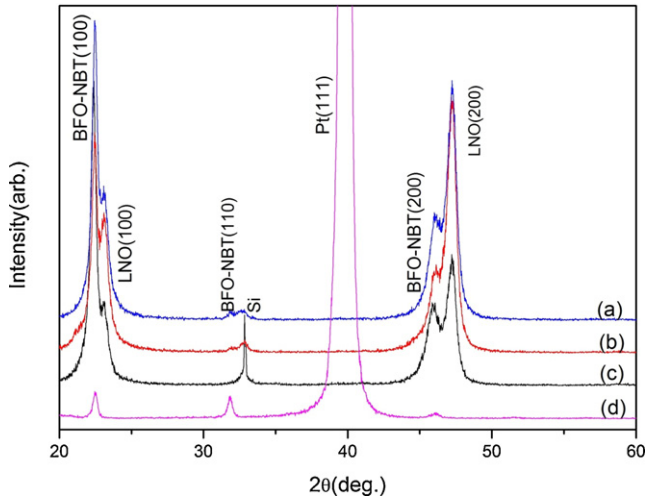

Fig. 1. The XRD patterns of $(1-x)$BFO–xNBT thin films deposited on SiO_2/Si substrates: (a) $x = 0.05$, (b) $x = 0.10$, (c) $x = 0.15$, and (d) the XRD pattern of films deposited directly on Pt substrates without LNO buffer layers ($x = 0.05$).

acid was added to promote alcoholysis. The solution was heated to 70 °C under constant stirring to obtain a stable and transparent solution. The concentrations of the solutions were adjusted to 0.15 M by adding 2-methoxyethanol. A two-step CSD process [27] was applied to deposit thin films. First, the solution was spin coated at 3500 rpm for 30 s. The as-deposited wet films were dried at 150 °C for 1 min and subsequently calcined at 350 °C for 5 min using a hot plate. Second, the films were annealed at 550 °C for 5 min in RTP-500 rapid thermal process furnace under the atmosphere of O_2. The spin coating and annealing procedures were repeated 10 times to obtain a desirable thickness.

XRD patterns were recorded using D/max2550VL/PC with Cu Kα radiation. The morphology of the films was observed with scanning electric microscopy (SEM) (JEOL-Japan). The optical properties were investigated via spectroscopic ellipsometry (W-VASE32TM Ellipsometer). In order to study the electrical properties of the films, Au top electrodes of 0.25 cm^2 and 0.09 cm^2 were deposited through a mask on the films by ion sputtering. The dielectric properties of the films were measured by impendence analyzer (HIOKI HiTESTER 3532-50) over 100 Hz to 100 kHz. Leakage currents were obtained using a KEITHLEY 6517B electrometer.

3. Results and discussion

The XRD patterns of the BFO–NBT thin films as shown in Fig. 1 indicate a pure perovskite structure of BFO–NBT thin films. From Fig. 1, XRD patterns (a)–(c) show that the BFO–NBT film on LNO substrate are well crystallized, showing strong diffraction peaks at around 22.4°and 46.0°, which correspond to the (1 0 0) and (2 0 0) reflections, respectively. This demonstrates a highly preferred orientation of BFO–NBT films along {1 0 0} direction. According to XRD patterns (a) and (d), an extremely high orientation degree of thin films is well achieved only when LNO buffer layers are applied. This may due to a lower energy growing along the (1 0 0) orientation, which is the result of heterogeneous nucleation owing to good lattice match between LNO buffer layers and BFO–NBT films. The estimated orientation degree of the film deposited is extremely high. The number of each $(1-x)$BFO–xNBT film is 97.6%, 97.7%, and 98.9% when x is 0.05, 0.10, and 0.15, respectively, according to equation $\alpha_{(100)} = I_{(100)}/(I_{(100)} + I_{(110)} + I_{(111)})$ [28]. The lattice parameter of BFO–NBT films obtained from XRD patterns using Bragg's law is 0.3659 nm, in agreement with previous reports of BFO films [3].

The cross-sectional and surface SEM images of the BFO–NBT films are presented in Fig. 2(a) and (b). In the cross-sectional image (a), a structure of columnar crystal was observed within the BFO–NBT films. The interfaces between BFO–NBT, LNO, and Si wafer are obvious and the thickness of BFO–NBT films is about 100 nm. From image (b), the grain size is estimated to be about 50 nm, and some relatively larger holes can be observed from the surface of the

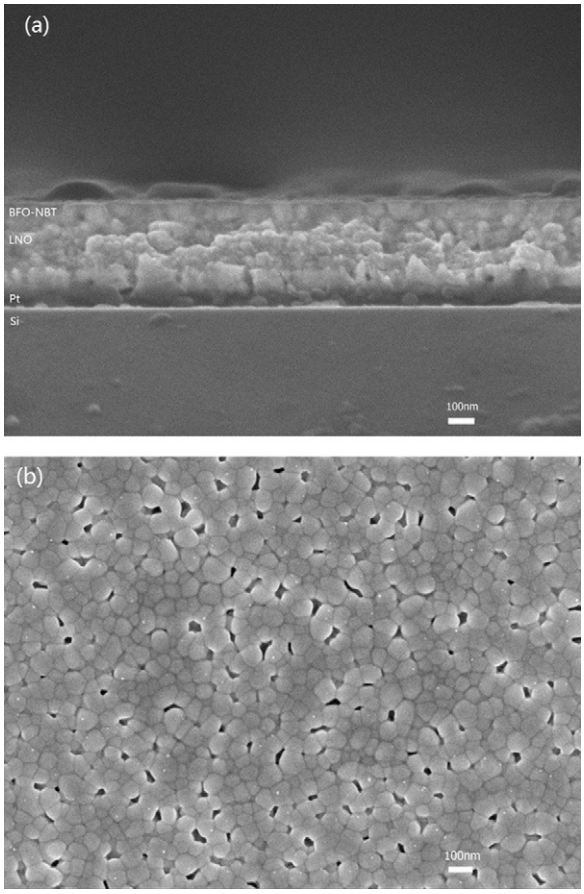

Fig. 2. SEM images of (a) cross-sectional structures and (b) surface structures of BFO–NBT thin films using LNO as buffer layers.

film grown on LNO layer, we also observed the surface of BFO–NBT films deposited on the Pt/Si/SiO_2 substrate (not shown). It exhibits a denser and more uniform surface. This indicates that it may be because the surface of the LNO layer is not uniform and with a relative larger number of holes, which then leads to an increase of the hole's density within BFO–NBT layers. As a result, it is of great necessity to improve the quality of LNO layers in order to reduce the defect density of BFO–NBT thin films. The average crystallite size of the films was also calculated according to Scherrer's equation $D = 0.9\lambda/\beta\cos\theta$ [29], which is estimated to be about 25 nm, where λ is the X-ray wavelength, β is the full width at half maximum (FWHM) in radians, and θ is the Bragg's angle. In general, the calculated value according to Scherrer's law is the crystallite size, which is usually smaller than the real grain size seen from SEM image [30].

The optical constants of the BFO–NBT films are derived from spectroscopic ellipsometry (SE) measurements at 400–1300 nm wavelength range with an angle of incidence of 70°. Experimental SE spectra were fitted based on the Cauchy–Urbach dispersion relation [31]. The optical constants: refractive index n and extinction coefficient k of the BFO–NBT films are displayed in Fig. 3. The refractive index and the extinction coefficient of the film is about 2.70 and 0.3 at 600 nm, 2.55 and less than 0.1 in the range of 800–1200 nm, respectively. Obviously, both n and k get smaller and eventually become stable as wavelength increases. It is concluded from absorption coefficient that the film has a strong absorption in the green and blue light range. The direct-band-gap energy E_g was estimated from Fig. 3 according to Tauc's law: $(\alpha h\nu)^2 = C(h\nu - E_g)$ [32]. The insets of absorption spectrums of Fig. 3(a)–(c) indicate a result that E_g of BFO–NBT thin film is around 2.74 eV, which can

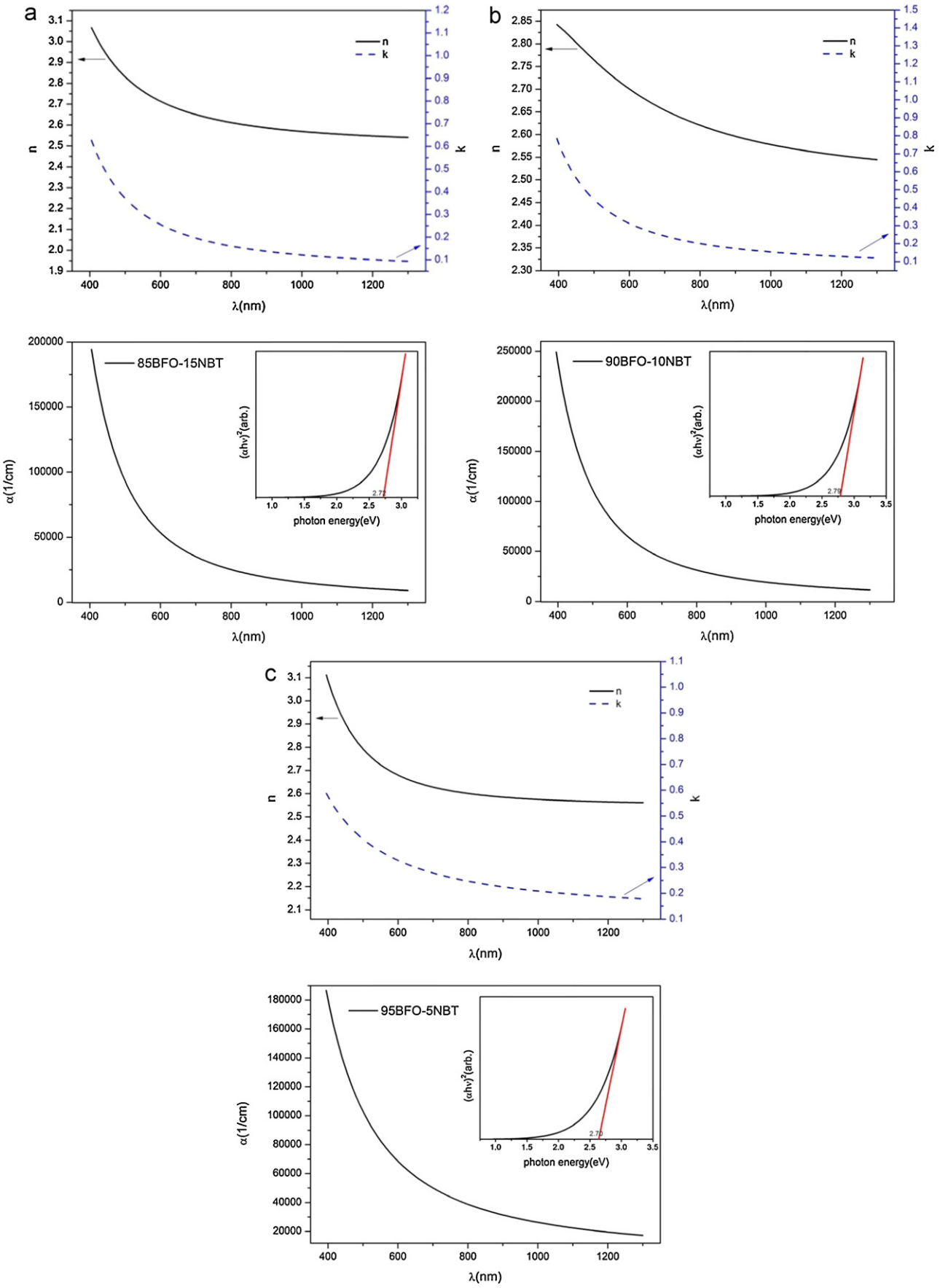

Fig. 3. Fitted refraction index, extinction coefficient, and absorption coefficient of $(1-x)$BFO–xNBT using data gained from spectroscopic ellipsometry: (a) $x = 0.15$, (b) $x = 0.1$, (c) $x = 0.05$ (insert diagram of absorption spectrum: $(\alpha h\nu)^2$ versus $h\nu$ plots of the $(1-x)$BFO–xNBT film).

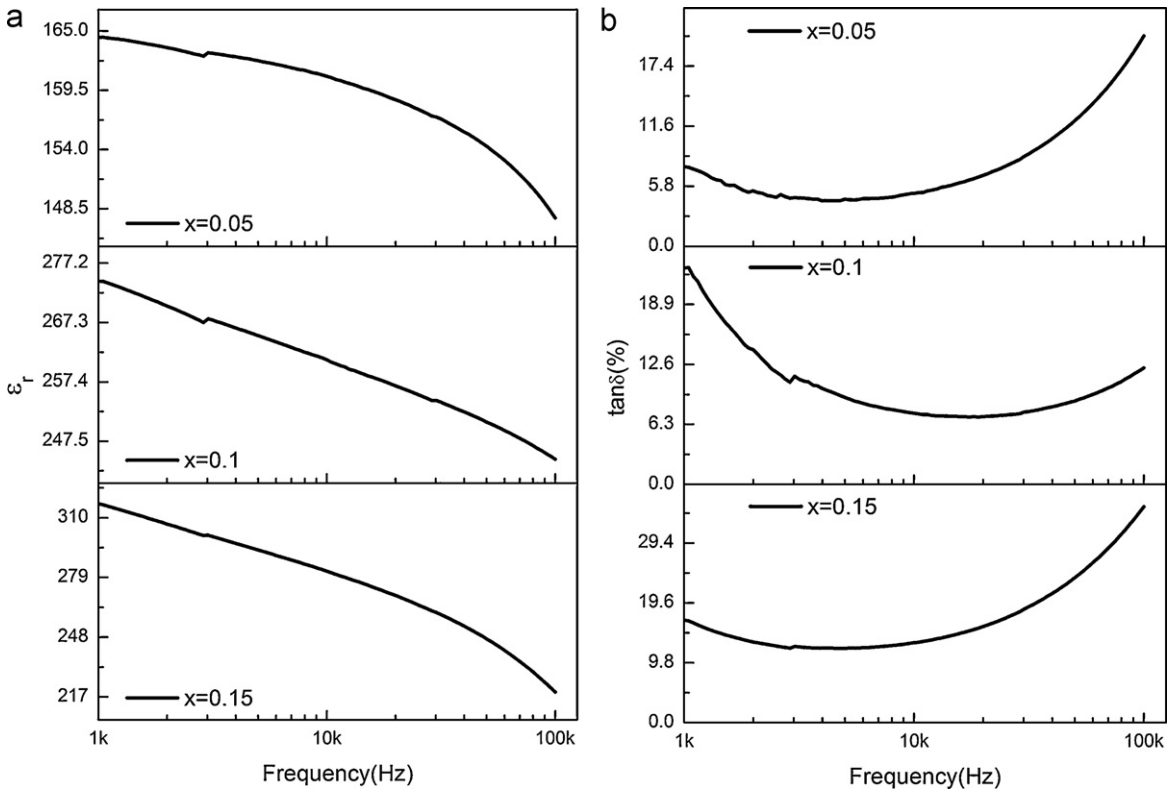

Fig. 4. (a) Dielectric constant ε_r and (b) dielectric loss tan δ dependent on frequency for $(1-x)$BFO–xNBT thin films at room temperature.

mainly be attributed to electron transition from the valence band to the conduction band. These results are well coordinate with previous work about BFO [33,34]. Also, the band-gap of BFO–NBT is slightly increased when more NBT was added.

Since the refractive index and band gap represent two fundamental physical aspects that characterize optical and electronic properties concerning the photovoltaic applications. The correlations between band gap and refractive index were also studied using an empirical relationship, $n^4(E_g - 0.365) = 154$, proposed by Reddy and Ahammed for semiconductors [35]. It is found that this equation is also in good agreement with our experiment result. This indicates the correlations of optical properties and electronic properties for BFO–NBT are similar to those of semiconductors, which provide us more perspectives in optoelectronic or photovoltaic applications for BFO–NBT thin films.

Fig. 4 shows the variation of the dielectric constant and dielectric loss as a function of frequency in the range of 1–100 kHz for the BFO–NBT thin films. The dielectric constant of the film decreases with the frequency increasing, which is approximately 54.2 at 1 MHz and 180.6 at 100 Hz. While ε_r of BFO is under 200 at 10 kHz [36], ε_r of NBT is over 400 under the same frequency [37]. Thus the dielectric constant increases with the change of x. A relatively low value of loss tangent was obtained for BFO–NBT films compared with the pure BFO thin film. The dielectric loss shows decrease at first and then increase with increasing the frequency. This phenomenon has been observed in many ferroelectric films. It is possibly due to an extrinsic resonance behavior resulting from the microstructure deficiency, which may be reduced by optimization of the film growth process.

Fig. 5 shows the J–E curves for the BFO–NBT films, measured at room temperature. All films exhibit a similar leakage current behavior, while much lower leakage current density is observed as the amount of NBT increased. As shown in the diagram, the leaking current is significantly suppressed from 1.26A cm^{-2} to 0.01 A cm^{-2} as more NBT was added when the applied bias voltage is 1.6 V. The leakage current density is related to the density of oxygen vacancies, which is generated by the deoxygenized Fe^{2+}. When NBT was introduced into the system, Ti^{4+} ions occupied the tetrahedral positions (TiO_4) or substitutional octahedral positions (TiO_6) [38,39] and therefore took the place of Fe^{3+} in BFO. The substitution of Fe^{3+} by Ti^{4+}could largely reduce the amount of deoxygenized Fe^{2+} and thereby prevent the generation of oxygen vacancies, where the oxygen vacancies should dominate the leakage behavior of BFO thin films. Thus a lower leakage current density is observed. The log–log plots of the leakage current density versus applied voltage of 85BFO–15NBT are shown in the inset of Fig. 5, and the curves can be divided into three regions. An Ohmic conduction behavior, which is dominated by thermally stimulated free electron conduction is demonstrated at low voltage (Region I). The leakage current during this period can be described by $J = n_0 q \mu AV/d$, where n_0 is the

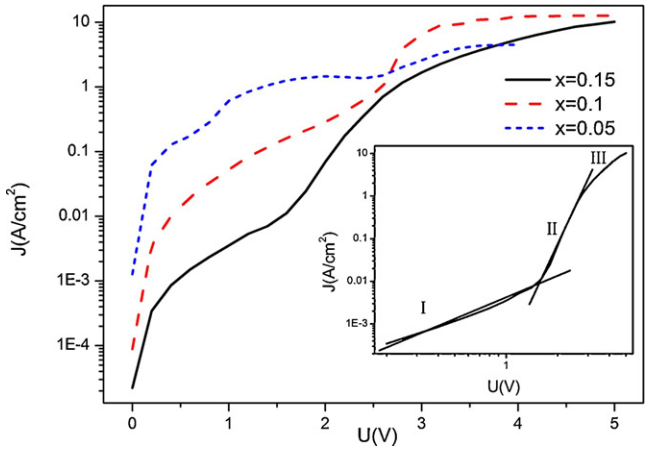

Fig. 5. The leakage currents of $(1-x)$BFO–xNBT (inset: log U versus log J of the leakage current of 85BFO–15NBT).

density of the thermally stimulated electrons, μ is the free carrier mobility, and A is the area of electrode. With higher voltage (Region II), the effect of space charge limited current (SCLC) takes the dominant part of the mechanism of the leakage current when charge carriers are captured by defects and oxygen vacancies. The SCLC current in a free trap is expressed by $J_{SCLC} = 9\varepsilon_r\varepsilon_0\mu AV^2/8d^3$, where ε_0 is the vacuum permittivity or the permittivity of free space, ε_r is the relative dielectric constant, μ is the ratio of thetotal density of free electrons to the trapped electrons, V is theapplied voltage, and d is the thickness of thin film [40]. The slope change between Regions I and II proves the transition from Ohmic to *SCLC* behavior. When the voltage continues to increase (Region III), Poole–Frenkel emission (PE) model takes place and further promotes the leakage current density. The PE is due to field-enhanced thermal excitation of electrons trapped because of SCLC behavior mentioned above from the insulator into the conduction band. The current density of which is given by $J = J_0 \exp((\beta_{PF}E^{1/2} - \Phi_{PF})/k_BT)$, where J_0 is the low-field current density, $\beta_{PF} = (e^3/\pi)^{1/2}$, Φ_{PF} is the height of trap potential well [41].

4. Conclusions

The preparation of BFO–NBT sol is studied. A stable precursor solution without precipitation is prepared. $(1-x)$BFO–xNBT thin films were deposited onto Si substrates with LNO as buffer layers via the sol–gel method. X-ray diffraction analyses show that the $(1-x)$BFO–xNBT films are highly (1 0 0)-oriented when LNO buffer layer is applied. Smooth surface with evenly distributed grains with a thickness of about 100 nm and grain sizes of about 50 nm were observed by scanning electron microscope. The dielectric, insulating characteristics, and optical properties of the films have been investigated. $(1-x)$BFO–xNBT thin films show a dielectric constant of 160–280 and a loss tangent of less than 10%. The films also display a good insulating characteristic against the applied field. The leaking current is significantly suppressed from 1.26 A cm^{-2} to 0.01 A cm^{-2} as the increase of NBT content when the applied bias voltage is 1.6 V. The film has a conspicuous absorption in the visible light region, and a band gap of about 2.74 eV. Our results indicate that the highly (1 0 0)-oriented $(1-x)$BFO–xNBT should be a promising candidate as the ferroelectric photovoltaic thin film material.

Acknowledgement

This work was supported by the National Natural Science Foundation of China (11074165).

References

[1] J. Wang, J.B. Neaton, H. Zheng, et al., Science 299 (2003) 1719.
[2] G. Catalan, J.F. Scott, Adv. Mater. 21 (2009) 2463.
[3] F. Zavaliche, S.Y. Yang, T. Zhao, et al., Phase Trans. 79 (2006) 991.
[4] R. Ramesh, N.A. Spaldin, Nat. Mater. 6 (2007) 21.
[5] T. Choi, S. Lee, Y.J. Choi, V. Kiryukhin, S.-W. Cheong, Science 324 (2009) 63.
[6] W. Ji, K. Yao, Y.C. Liang, Adv. Mater. 22 (2010) 1763.
[7] C. Bin, M. Li, Y. Liu, Z. Zuo, F. Zhuge, Q. Zhan, R. Li, Nanotechnology 22 (2011) 195201.
[8] D.K. Mishra, X. Qi, J. Alloys Compd. 504 (2010) 27.
[9] H. Huang, Nat. Photonics 4 (2010) 134.
[10] M. Ichiki, Y. Morikawa, T. Nakada, R. Maeda, Ceram. Int. 30 (2004) 1831.
[11] W.C. Wang, H.W. Zheng, X.Y. Liu, X.S. Liu, Y.Z. Gu, H.R. Zhang, W.F. Zhang, Chem. Phys. Lett. 488 (2010) 50.
[12] Y. Zang, D. Xie, X. Wu, Y. Chen, Y. Lin, M. Li, H. Tian, X. Li, Z. Li, H. Zhu, T. Ren, D. Plant, Appl. Phys. Lett. 99 (2011) 132904.
[13] T.L. Qu, Y.G. Zhao, D. Xie, J.P. Shi, Q.P. Chen, T.L. Ren, Appl. Phys. Lett. 98 (2011) 173507.
[14] S.Y. Yang, J. Seidel, S.J. Byrnes, et al., Nat. Nano 5 (2010) 143.
[15] M. Alexe, D. Hesse, Nat. Commun. 2 (2011) 256.
[16] A.M. Glass, D. von der Linde, T.J. Negran, Appl. Phys. Lett. 25 (1974) 233.
[17] M. Ichiki, R. Maeda, Y. Morikawa, Y. Mabune, T. Nakada, K. Nonaka, Appl. Phys. Lett. 84 (2004) 395.
[18] M. Ichiki, H. Furue, T. Kobayashi, R. Maeda, Y. Morikawa, T. Nakada, K. Nonaka, Appl. Phys. Lett. 87 (2004) 222903.
[19] J. Wu, J. Wang, Electrochem. Solid State Lett. 13 (2010) G105.
[20] D.Y. Wang, N.Y. Chan, R.K. Zheng, C. Kong, D.M. Lin, J.Y. Dai, H.L.W. Chan, S. Li, J. Appl. Phys. 109 (2011) 114105.
[21] G.A. Smolensky, V.A. Isupov, A.Y. Agranovskaya, N.N. Krainik, Sov. Phys. Solid State 2 (1961) 2651.
[22] V. Dorcet, P. Marchet, G. Trolliard, J. Eur. Ceram. Soc. 27 (2007) 4371.
[23] E. Venkata Ramana, S.V. Suryanarayana, T. Bhima Sankaram, Solid State Sci. 12 (2010) 956.
[24] H. Miyazaki, T. Goto, Y. Miwa, T. Ohno, H. Suzuki, T. Ota, M. Takahashi, J. Eur. Ceram. Soc. 24 (2004) 1005.
[25] R.W. Schwartz, Chem. Mater. 9 (1997) 2325.
[26] R.W. Schwartz, T. Schneller, R. Waser, C. R. Chimie 7 (2004) 433.
[27] Y. Guo, K. Suzuki, K. Nishizawa, T. Miki, K. Kato, J. Cryst. Growth 284 (2005) 190.
[28] C. Cho, W. Lee, B. Yu, B. Kim, J. Appl. Phys. 86 (1999) 2700.
[29] A.L. Patterson, Phys. Rev. 56 (1939) 978.
[30] Y. Guo, K. Suzuki, K. Nishizawa, T. Miki, K. Kato, Jpn. J. Appl. Phys. 45 (2006) 855.
[31] F. Atay, V. Bilgin, I. Akyuz, E. Ketenci, S. Kose, J. Non-Cryst. Solids 356 (2010) 2192.
[32] T.D. Kang, H. Lee, S.J. Park, J. Jang, S. Lee, J. Appl. Phys. 92 (2002) 2467.
[33] J.F. Ihlefeld, N.J. Podraza, Z.K. Liu, R.C. Rai, X. Xu, T. Heeg, Y.B. Chen, J. Li, R.W. Collins, J.L. Musfeldt, X.Q. Pan, J. Schubert, R. Ramesh, D.G. Schlom, Appl. Phys. Lett. 92 (2008) 142908.
[34] X.S. Xu, T.V. Brinzari, S. Lee, et al., Phys. Rev. B 79 (2009) 134425.
[35] R.R. Reddy, Y. Nazeer, Ahammed, Infrared Phys. Technol. 36 (1995) 825.
[36] T.P. Gujar, V.R. Shinde, S.S. Kulkarni, H.M. Pathan, C.D. Lokhande, Appl. Surf. Sci. 252 (2006) 3585.
[37] J. Xu, Y. Liu, R.L. Withers, F. Brink, H. Yang, M. Wang, J. Appl. Phys. 104 (2008) 116101.
[38] T. Satyanarayana, I.V. Kityk, K. Ozga, M. Piasecki, P. Bragiel, M.G. Brik, V. Ravi Kumar, A.H. Reshak, N. Veeraiah, J. Alloys Compd. 482 (2009) 283.
[39] G.M. Krishna, N. Veeraiah, N. Venkatramaiah, R. Venkatesan, J. Alloys Compd. 450 (2008) 477.
[40] Y. Guo, D. Akai, K. Sawada, M. Ishida, Solid State Sci. 10 (2008) 928.
[41] M.C. Kao, H.Z. Chen, S.L. Young, Mater. Lett. 62 (2008) 629.